Formation of a reliable intermediate band in Si heavily coimplanted with chalcogens (S, Se, Te) and group III elements (B, Al)

K. Sánchez, I. Aguilera, P. Palacios, and P. Wahnón[*]

Instituto de Energía Solar y Departamento de Tecnologías Especiales, ETSI Telecomunicación, UPM–Ciudad Universitaria, Madrid 28040, Spain

This first-principles study describes the properties of Si implanted with several chalcogen species (S, Se, Te) at doses considerably above the equilibrium solubility limit, especially when coimplanted with the group III atoms B and Al. The measurements of chalcogen-implanted Si show strong optical absorption in the infrared range. The calculations carried out show that substitution of Si by chalcogen atoms requires lower formation energy than the interstitial implantation. In the resulting electronic structure, at concentrations close to 0.5%, an impurity band determined by the properties of the chalcogens introduced is observed in the forbidden energy gap of Si. Although this band is a few tenths of an electron volt wide, it remains energetically isolated from both the valence and the conduction bands. Appropriate coimplantation with group III elements allows control over the occupation of the intermediate band while modifying its energies only slightly. A moderate energy gain (especially small for B) seems to be obtained when p-doping atoms occupy the sites next to those of the chalcogens. Therefore, the apparent electrostatic attraction between species that in isolation would act as acceptors and double donors is smaller than expected. The intermediate-band properties have been preserved for all of the coimplanted compounds analyzed here, regardless of the species involved or the distance between them, which constitutes an appreciable advantage for the design of new experimental materials.

I. INTRODUCTION

Recently, it has been proposed that the properties of crystalline intermediate-band materials derived from Si may allow for the development of an operating intermediate-band solar cell in the near future.[1,2] An intermediate-band material is characterized by an electronic band [the so-called intermediate band (IB)] placed within the band gap of a host semiconductor that remains energetically isolated from both the valence and the conduction bands (VB and CB, respectively).[3] Its partial occupation allows absorbed low-energy photons to produce additional photogenerated carriers. It is expected that once an adequate combination of host semiconductor and introduced transition metal is achieved, the quantum efficiency of IB solar cells will be considerably enhanced.[4–8] Si-based IB materials could also allow easier and faster device manufacture. Experimental growth, corroboration of the atomic structure, and electrical characterization of experimental samples of Ti-implanted Si at very high concentrations has been done in an attempt to develop materials that can be used to construct an IB solar cell in the future.[1,9–11] Pulsed laser irradiation, when applied over Si in the presence of gases such as SF_6, can produce compounds that have enhanced properties.[12] The resulting material, so-called black silicon, presents strong optical absorption even at energies below the Si band gap. Near-unity absorptance has been found for photon energies down to approximately 0.5 eV.[13] Furthermore, crystallinity of sulfur-implanted material has been observed even at S concentrations near 0.5%, which is several orders of magnitude above its solid solubility.[14] This concentration is also expected to far surpass the so-called Mott limit.[15] Therefore, it is expected that some of the electrons from the implanted atoms interact and form a band, rather than behaving as if they belonged to isolated

impurities. Similar work on Si implanted and annealed with other chalcogen species, such as Se and Te, has been presented elsewhere.[16,17] Their characterization showed that these compounds also present subband-gap absorption features. Several analogies observed in the fabrication procedure and the properties of chalcogen-implanted and Ti-implanted Si compounds have encouraged research devoted to obtaining a photovoltaic material with an IB in its electronic structure. In this paper, we will describe how the introduction of chalcogen atoms can produce an IB material upon coimplantation with group III elements and we will demonstrate the robustness of IB band properties in these compounds. In the next section, the first-principles method used will be briefly outlined. Afterward, the results including the atomic structure, energetics, electronic properties, and optical characterization of intrinsic and p-doped chalcogen-implanted Si will be presented and discussed. Finally, the summary and conclusions drawn from the obtained results will be explained.

II. METHOD

The first-principles calculations carried out in this work are based on the density-functional theory.[18,19] Plane-wave-based VASP computational code[20,21] was employed. The generalized gradient approximation (GGA) through the PW91 functional[22] was used to take into account the exchange-correlation potential. Core electrons were represented by means of the projector augmented wave potentials.[23,24]

The concentration of implanted chalcogen atoms achieved in the experimental samples surpassed 10^{20} cm^{-3}. Therefore, the unit cells considered in this study were derived from the $3 \times 3 \times 3$-Si$_8$ cubic supercell to obtain compounds with a similar dilution level. All of the atomic structures analyzed

were relaxed using thresholds of 0.01 eV/Å for the inter-atomic forces and 0.1 GPa for the lattice stress. A quasi-Newton algorithm was used to relax the ions and the cell parameters. In this method the stress tensor and the forces determine the search direction by calculating the Hessian matrix so a good set of relaxed forces must be obtained.[25]

To estimate the formation energies of the compounds that will be presented below, only the most stable phase of each element was used as a reactant. Only compounds with one chalcogen atom per formula were taken into account, which allows direct comparison of the relative stability of the different compounds. To get an overview of the possible formation of dimers, calculations involving the substitution of two nearest neighbors of Si by S were carried out. The relaxation evolved to a separation between both S atoms as was previously found in the bibliography.[26,27] Therefore the S_2 dimer formation seems unlikely.

A Γ-centered $4 \times 4 \times 4$ Monkhorst-Pack grid of reciprocal lattice points was used to sample the irreducible Brillouin zone. The Methfessel-Paxton first-order scheme[28] with 0.1 eV of smearing was used to obtain the occupations of Kohn-Sham eigenvalues. The well-known underestimation of the Si band gap obtained by the GGA approach is corrected in this work by applying a scissor operator over the empty states to recover the experimental band gap of the host semiconductor. The value of the shift necessary to match the 1.12 eV of the bulk Si band gap corresponds to 0.49 eV, as used in the analogous case of Ti-implanted Si.[2]

Optical properties were obtained from the dielectric function using the OPTICS code written by Furthmüller.[29] While its imaginary part is calculated from a sum over independent transitions between Kohn-Sham states neglecting local field effects,[30] the real part was obtained from the imaginary part making use of the Kramers-Kronig relations. Approximately 250 empty bands and a $\Gamma-8 \times 8 \times 8$ sampling of the Brillouin zone were needed to assess the convergence of the optical properties.

III. RESULTS

A. Chalcogen-implanted Si

1. Electronic and energetic properties

Substitution of one Si atom by S (S_{Si}) in the 216-atom cell produces no significant changes in the atomic structure. The electronic density of states (DOS) that results from the application of the rigid shift is shown in Fig. 1(a). An occupied band, corresponding to the deep levels of sulfur, appears within the Si band gap. In contrast to a number of previous candidates for IB material,[4–8] this compound does not show any possible ferromagnetic ordering even at zero temperature. This difference is due to the absence of transition metals in the compound. Taking into account the underestimation of the band gap by 0.49 eV, the band is assumed to be placed 0.39 eV above the VB maximum and 0.51 eV below the CB minimum. It is 0.22 eV wide and therefore the band gap of the host semiconductor is not modified (see Table I).

To study another possible situation of the implantation process, the atomic structure of *interstitial* sulfur with for-
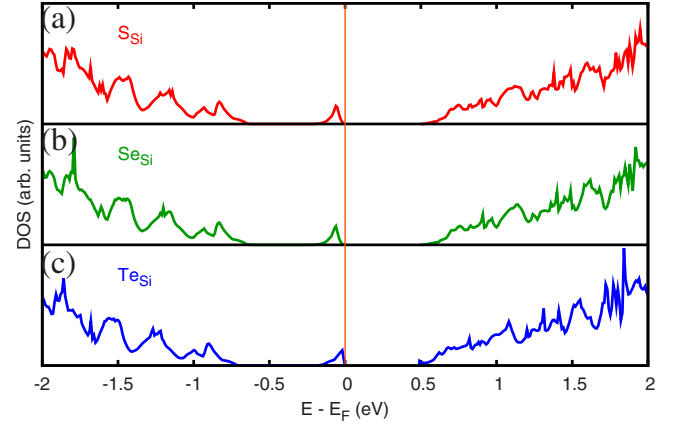

FIG. 1. (Color online) Density of states diagrams obtained for the relaxed (a) $S_{Si}Si_{215}$, (b) $Se_{Si}Si_{215}$, and (c) $Te_{Si}Si_{215}$.

mula S_iSi_{216} was optimized. Four Si nearest neighbors are sited at 2.41–2.42 Å, forming a tetrahedral coordination while six second-nearest neighbors are placed in an octahedral configuration at 2.81–2.82 Å. The subsequent DOS diagram is presented in Fig. 2. In contrast to the case of Ti-implanted Si,[2] the S_iSi_{216} compound is not considered to be a promising candidate for a IB material. Although the bands that appear present interesting features, the lower one overlaps with the VB of the host semiconductor.

Corresponding synthesis reactions for both sulfur implantations were derived from bulk Si and the orthorhombic (α) phase of sulfur, which is the most stable phase known for this element

$$E^f[S_{Si}Si_{215}] = E[S_{Si}Si_{215}] - \left(\frac{1}{128}\right)E[S_{128}] - \left(\frac{215}{216}\right)E[Si_{216}]$$

$$= -0.13 \text{ eV},$$

$$E^f[S_iSi_{216}] = E[S_iSi_{216}] - \left(\frac{1}{128}\right)E[S_{128}] - E[Si_{216}]$$

$$= +2.71 \text{ eV}.$$

In view of the calculations showing an energy difference of 2.84 eV per S atom between the two formation processes, it is predicted that interstitial implantation of sulfur is considerably less stable than substitutional positioning. Initially, the negative formation energy was attributed to the difficulty in accurately calculating the total energy of α-S. In this compound, Van der Waals forces between S_8 rings, which are absent in GGA calculations, would further stabilize the en-

TABLE I. Summary of the bandwidth and forbidden energy gaps of the chalcogen-implanted compounds. All values are given in eV.

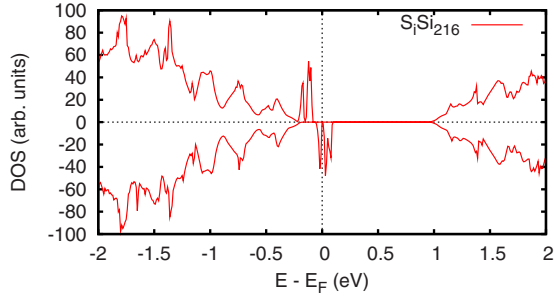| Compound	IB bandwidth	ΔE[VB-IB]	ΔE[IB-CB]	ΔE[VB-CB]
$S_{Si}Si_{215}$	0.22	0.39	0.51	1.12
$Se_{Si}Si_{215}$	0.22	0.40	0.50	1.12
$Te_{Si}Si_{215}$	0.25	0.47	0.38	1.10

FIG. 2. (Color online) Density of states diagrams obtained for the relaxed $S_i Si_{216}$.

ergy of the crystal. Therefore, the sulfur energy was estimated using a method that consists of inverting the formation reaction of silicon sulfide (SiS), for which the experimental enthalpy at zero temperature is known $[\Delta H_f^0[SiS] = -104.65$ kJ/mol (Ref. 31)]

$$E[S] = E[SSi] - \left(\frac{1}{128}\right)E[Si_{216}] - \Delta H_f^0[SiS] = -4.03 \text{ eV}.$$

Introducing this value into the formation reaction of $S_{Si}Si_{215}$ resulted in an energy balance of -0.16 eV, which is in agreement with the aforementioned result obtained exclusively from DFT calculations. In selenium-implanted Si ($Se_{Si}Si_{215}$), Se atoms are arranged with Si at an interatomic distance of 2.57 Å. This distance is a bit longer than the corresponding distance for sulfur, as was expected. The formation energy of the Se substitution is calculated by taking the trigonal γ phase for the Se reactant

$$E^f[Se_{Si}Si_{215}] = E[Se_{Si}Si_{215}] - \left(\frac{1}{3}\right)E[Se_3] - \left(\frac{215}{216}\right)E[Si_{216}]$$

$$= +1.29 \text{ eV}.$$

In contrast to the case for sulfur, the stable phase of selenium does not include Van der Waals interactions and therefore the value obtained is more trustworthy. It is, although positive, still lower than the formation energy obtained for $Ti_{Si}Si_{215}$.[2] Therefore, because crystalline Si supersaturated with Ti has already been synthesized successfully,[1] it is highly likely that Se-implanted samples with similar concentrations can be produced in the laboratory. Indeed, fabrication of Se-implanted Si with a concentration of 0.1% has been already carried out.[16]

The DOS diagram for $Se_{Si}Si_{215}$, presented in Fig. 1(b), is almost identical to that of the S-substituted compound, which is not surprising given that the experimental impurity levels of these chalcogens differ by less than 0.02 eV.[32] The IB is 0.22 eV wide and it is placed 0.40 eV above the VB and 0.50 eV below the CB (see Table I).

In the case of $Se_i Si_{216}$, the DOS diagram (not shown) is qualitatively equal to $S_i Si_{216}$ DOS. Only a smaller energy separation between the IB and the VB is found so a minor increase in the selenium concentration could increase the IB width and cause an overlap with the VB. Furthermore, the energy balance shown below suggests that the formation reaction of this compound is quite unfavorable

$$E^f[Se_i Si_{216}] = E[Se_i Si_{216}] - \left(\frac{1}{3}\right)E[Se_3] - E[Si_{216}]$$

$$= +5.06 \text{ eV}.$$

In this case, the difference in the formation energy between the interstitial and substitutional implantations is 3.77 eV per atom introduced, even larger than that calculated for sulfur, suggesting that Se atoms will mostly substitute Si. Therefore, although several analogies are found between the electronic properties of $S_{Si}Si_{215}$ and $Se_{Si}Si_{215}$, differences in the size of the chalcogen atom determine the differences in the energetics and the structures.

For tellurium-implanted material the interatomic distance is even longer than in the Se-implantation case. Formation energy for a hypothetical reaction obtained from the trigonal stable phase of Te is

$$E^f[Te_{Si}Si_{215}] = E[Te_{Si}Si_{215}] - \left(\frac{1}{3}\right)E[Te_3] + \left(\frac{215}{216}\right)E[Si_{216}]$$

$$= +1.97 \text{ eV}.$$

Therefore, the increase in the size of the substituting atom discourages the substitution more than for the other chalcogens. Furthermore the DOS diagram is qualitatively similar to $S_{Si}Si_{215}$. The only difference is the Te defect level which is slightly wider than S and Se ones. In addition, its position is closer to the CB than those of the chalcogens analyzed above (Table I).

The calculation of the structure for the interstitial implantation of Te failed to show relaxation beyond the convergence thresholds for atomic forces and energy, which may be due to the large size of Te, which prevents its adaptation to the Si interstitials. There are two factors that support this reasoning: first, the energy difference between substitutional and interstitial implantation increases with the size of the chalcogen; second, the introduction of larger chalcogen atoms causes considerably greater distortions in the interstitially implanted lattices.

Summarizing, several common features can be extracted from the results analyzed above. A relatively narrow band appears within the band gap for all of the chalcogen substitutions. This band consists of one state per spin channel and both states are fully occupied.

The energy variation in the appearing band regarding the change in the chalcogen species of $X_{Si}Si_{215}$ resembles to some extent the relationship existing between the chalcogen donor levels. However, the intention of this report is not to compare the energy position of discrete impurity levels in a crystalline compound (which furthermore were already calculated theoretically[33–35] and observed experimentally[32,36,37]) but to verify if the chalcogen substitution at such concentration level produces a band with initial width and energies according to the expected for an intermediate-band material.

To reduce the population of this band, coimplantation with elements belonging to group III is proposed. In principle, some variation in the band energies could be expected after coimplantation. However, in this case, no overlap with the host semiconductor band edges is forecasted because the bands obtained for the chalcogen-substituted Si appear at the
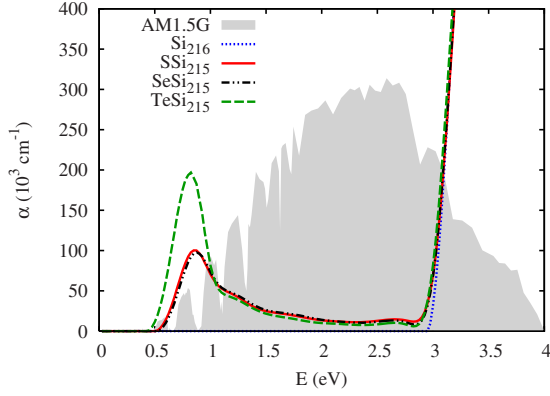
FIG. 3. (Color online) Optical absorption coefficient calculated for $S_{Si}Si_{215}$, $Se_{Si}Si_{215}$, and $Te_{Si}Si_{215}$ compounds compared to that of pure Si. The AM1.5G solar spectrum (Ref. 38) in the background is shown as a reference.

central region of the Si band gap. These properties will be further analyzed in Sec. III B.

2. Optical properties

Because of the difference in the formation energies of both kinds of implantation, only the optical properties of the substitutional cases will be analyzed. The absorption coefficients of $S_{Si}Si_{215}$, $Se_{Si}Si_{215}$, and $Te_{Si}Si_{215}$ are presented and compared to that of pure Si in Fig. 3. A sizable contribution from the transitions involving the IB at energies below the direct gap is observed in all cases. The main peak appears at 0.8 eV and is approximately 0.2 eV wide. In the case of $Se_{Si}Si_{215}$, this result agrees quite well with a report that identified the peak of experimental absorptance at 1800 nm.[16] The agreement between these values supports our method for calculating the optoelectronic properties of the material, despite the apparent simplicity of relying on the rigid shift.

In the absorption coefficient of $Te_{Si}Si_{215}$, the peak appears at energies close to 0.8 eV as well, although in this case its size is larger than that of the other chalcogen implantations studied. This larger peak is because the energies of the Te levels are slightly closer to the CB, and therefore, the probability of the photoelectric effect (which varies roughly as a
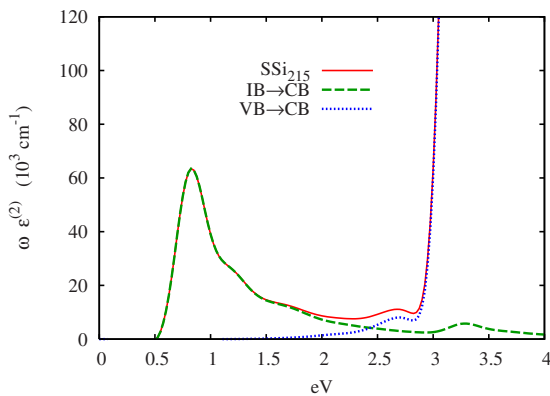

FIG. 4. (Color online) Imaginary part of the dielectric function calculated for the $S_{Si}Si_{215}$ compound separated into the contributions of the two possible absorption processes.
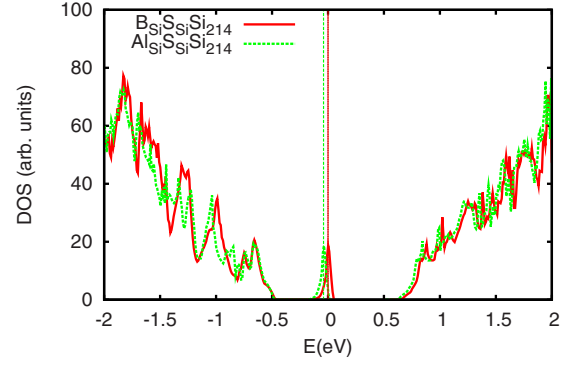

FIG. 5. (Color online) Density of states diagrams obtained for the remotely coimplanted $B_{Si}S_{Si}Si_{214}$ (red solid) and $Al_{Si}S_{Si}Si_{214}$ (green dotted). Vertical lines indicate the Fermi energies of both compounds.

cubic function with the photon energy) is substantially higher when the energy gap between full and empty states decreases.

At higher energies (up to the direct band gap of Si and beyond), optical absorption is also predicted for the three compounds, although it is a secondary feature compared with the 0.8 eV peak. To see how the intermediate band contributes to the total absorption coefficient, we have separated, in Fig. 4, the partial contributions to absorption of $S_{Si}Si_{215}$, using the imaginary part of the dielectric function $\varepsilon^{(2)}$.

The main peak at 0.8 eV is associated with the electronic transitions from the IB to the lowest energy levels of the CB. This observation is supported by the similarity between the peak width and the band dispersion as well as by the agreement between the position of the peak and the energy difference between the electronic bands. The contribution from the IB to the CB decreases at higher energies and forms a tail. The same behavior was found for $Se_{Si}Si_{215}$ and $Te_{Si}Si_{215}$, as was expected in view of the similar electronic structures obtained.

B. Coimplantation with group III elements

1. Electronic and energetic properties

A compound with the formula $B_{Si}S_{Si}Si_{214}$ is obtained from coimplantation with boron at the same concentration as that of sulfur. After placing both substituting atoms at remote

TABLE II. Summary of the bandwidth and forbidden energy gaps of S-implanted compounds upon coimplantation with B or Al. All values are given in eV.

$B_{Si}S_{Si}Si_{214}$	IB bandwidth	ΔE[VB-IB]	ΔE[IB-CB]	ΔE[VB-CB]
Remote	0.21	0.29	0.58	1.08
Close	0.23	0.42	0.46	1.11

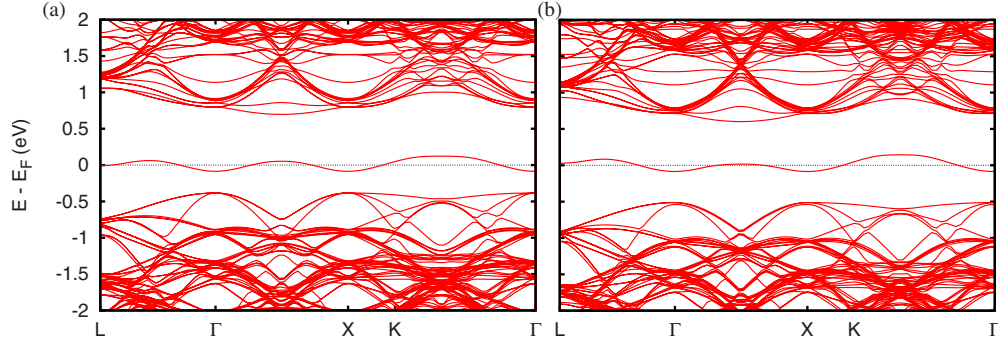| $Al_{Si}S_{Si}Si_{214}$	IB bandwidth	ΔE[VB-IB]	ΔE[IB-CB]	ΔE[VB-CB]
Remote	0.21	0.26	0.59	1.06
Close	0.22	0.45	0.43	1.10

FIG. 6. (Color online) The electronic band structure for (a) remotely and (b) closely coimplanted $B_{Si}S_{Si}Si_{214}$.

(R) positions, the calculated formation energy for $B_{Si}S_{Si}Si_{214}^R$ is

$$E^f[B_{Si}S_{Si}Si_{214}^R] = E[B_{Si}S_{Si}Si_{214}^R] - \left(\frac{214}{216}\right)E[Si_{216}]$$
$$- \left(\frac{1}{36}\right)E[B_{36}] - \left(\frac{1}{128}\right)E[S_{128}]$$
$$= -0.49 \text{ eV}.$$

The DOS diagrams obtained for the $B_{Si}S_{Si}Si_{214}$ and $Al_{Si}S_{Si}Si_{214}$ compounds are shown in Fig. 5. If the latter is compared with the $S_{Si}Si_{215}$ DOS diagram [Fig. 1(a)], it can be observed that the most noticeable effect of the B and Al implantation is the reduction in the band occupation down to half-filled. Therefore, the remaining requirement for an IB material, that is, the simultaneous presence of both electrons and holes in the band, is now accomplished. The main difference between B and Al codoping is that the energy of the VB maximum is slightly higher for the latter. As a result, the subband gap between VB and IB and the host semiconductor gap are slightly reduced (see Table II). These small changes in both energies are due to Al's shallower experimental acceptor level (0.072 eV) compared to B (0.045 eV).

In contrast to a number of previous candidates including doping with transition metals,[2,4–7] the electronic structure of this IB material remains paramagnetic, even upon coimplantation, probably because of the absence of transition metals in the atomic structure. The resulting IB has a width similar to that obtained without coimplantation, although the presence of B produces a slight negative displacement of the band (roughly a tenth of an electron volt). The shallow-acceptor character of boron also reduces the band gap of the host semiconductor down to 1.08 eV in the calculations (see Table II).

If two neighboring Si atoms are substituted by S and B, the resulting electronic structure [Fig. 6(b)] does not change significantly from the remote configuration [Fig. 6(a)]. A half-filled IB appears again inside the host semiconductor gap. However, in this case both subband gaps have similar values, and therefore the band is located almost in the middle of the host semiconductor gap. As a result, coimplantation of B and S atoms results in retained IB energies similar to those of the $S_{Si}Si_{215}$ compound. The total energy of this so-called

close (C) configuration is 0.14 eV lower than that of the remote structure

$$E^f[B_{Si}S_{Si}Si_{214}^C] = E[B_{Si}S_{Si}Si_{214}^C] - \left(\frac{214}{216}\right)E[Si_{216}]$$
$$- \left(\frac{1}{36}\right)E[B_{36}] - \left(\frac{1}{128}\right)E[S_{128}]$$
$$= -0.64 \text{ eV}$$

probably because the B radius is shorter than the Si radius while the S radius is longer. Therefore, at long enough distances, both effects can cancel. Interatomic distances are somewhat affected by the relative position of both atoms. The distance from B to the three Si atoms is 2.03 Å and the S-Si distance is also reduced, from 2.48 to 2.36 Å. However, the B-S distance obtained is 2.95 Å, a value slightly higher than expected taking into account the atomic radii of these species. The similarity between the energies above suggests that although boron is a shallow acceptor and sulfur usually behaves as a double donor, the electrostatic attraction between both implanted species is not very intense.

Furthermore, the resemblance between the band structures obtained in Figs. 6(a) and 6(b) suggests that, in principle, the tendency of both elements to localize next to each other does not alter the character of $B_{Si}S_{Si}Si_{214}$ as an IB material. In the rest of this section the discussion will be only focused on the remote dopant cases.
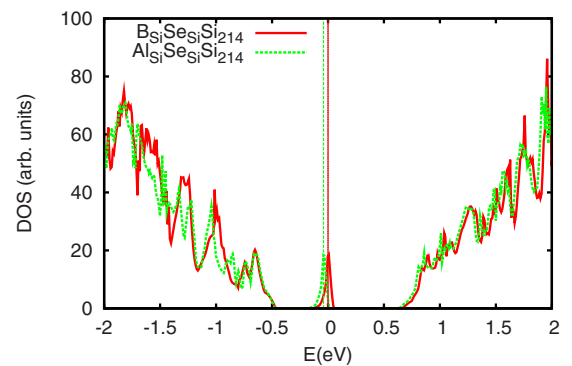

FIG. 7. (Color online) Density of states diagrams obtained for the remotely coimplanted $B_{Si}Se_{Si}Si_{214}$ (red solid) and $Al_{Si}Se_{Si}Si_{214}$ (green dotted).

TABLE III. Summary of the bandwidth and forbidden energy gaps for Se-implanted compounds upon coimplantation with B or Al. All values are given in eV.

$B_{Si}Se_{Si}Si_{214}$	IB bandwidth	ΔE[VB-IB]	ΔE[IB-CB]	ΔE[VB-CB]
Remote	0.21	0.29	0.59	1.09

$Al_{Si}Se_{Si}Si_{214}$	IB bandwidth	ΔE[VB-IB]	ΔE[IB-CB]	ΔE[VB-CB]
Remote	0.21	0.26	0.60	1.07

TABLE IV. Summary of the bandwidth and forbidden energy gaps of the Te-implanted compounds upon coimplantation with B or Al. All values are given in eV.

$B_{Si}Te_{Si}Si_{214}$	IB bandwidth	ΔE[VB-IB]	ΔE[IB-CB]	ΔE[VB-CB]
Remote	0.23	0.42	0.42	1.07

$Al_{Si}Te_{Si}Si_{214}$	IB bandwidth	ΔE[VB-IB]	ΔE[IB-CB]	ΔE[VB-CB]
Remote	0.24	0.39	0.42	1.05

When the $Se_{Si}Si_{215}$ compound is coimplanted with B substituting for Si, the obtained IB is also half-filled (see Fig. 7), as shown for the compound containing sulfur. As a secondary effect, the band that appears for $B_{Si}Se_{Si}Si_{215}^R$ is slightly displaced to energies 0.1 eV higher than those of the band structure for $Se_{Si}Si_{215}$ (Table III). Therefore, the results and the effect of coimplantation resemble those found for the compounds containing sulfur.

The formation energy of $B_{Si}Se_{Si}Si_{214}$ structure shows a negative value

$$E^f[B_{Si}Se_{Si}Si_{214}^R] = E[B_{Si}Se_{Si}Si_{214}^R] - \left(\frac{214}{216}\right)E[Si_{216}]$$
$$- \left(\frac{1}{36}\right)E[B_{36}] - \left(\frac{1}{128}\right)E[Se_3]$$
$$= -0.45 \text{ eV}$$

but it is positive for $Al_{Si}Se_{Si}Si_{214}^R$ ($E^f[Al_{Si}Se_{Si}Si_{214}^R] = +1.64$ eV). Therefore, when coimplanting with Se, it should be easier to obtain a homogeneous distribution of B atoms than of Al atoms.

Coimplantation of $Te_{Si}Si_{215}$ with group III elements produces results that are qualitatively similar to those obtained for the preceding chalcogens (Fig. 8). Previous trends are reproduced despite small quantitative differences (see Table IV). The latter are caused by the former $Te_{Si}Si_{215}$ electronic structure, which is in turn related to the impurity levels of Te.

The coimplantation cases evaluated in Fig. 8 show that it is possible to introduce holes in the IB without causing it to
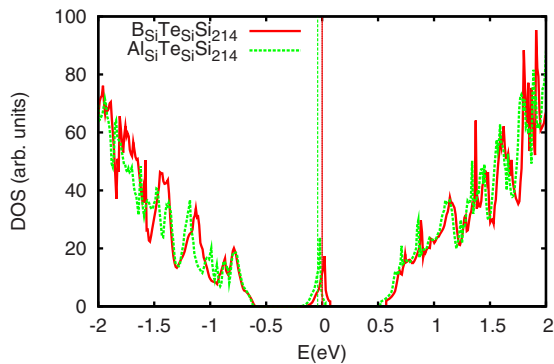

FIG. 8. (Color online) Density of states diagrams obtained for the remotely coimplanted $B_{Si}Te_{Si}Si_{214}$ (red solid) and $Al_{Si}Te_{Si}Si_{214}$ (green dotted).

overlap with the host semiconductor bands. The only noticeable effect consists of a small displacement to lower (higher) energies when *X*- and Te-substituting atoms are placed in remote (close) sites. The structures obtained upon relaxation also provide interatomic distances close to those expected and there are no significant deviations from the trends established by the aforementioned compounds. Energy calculations obtained using a similar procedure to those described in the aforementioned cases show that the formation energy of $B_{Si}Te_{Si}Si_{214}^R$ (+0.15 eV) is higher than the corresponding to the other dopants

In summary, the electronic properties of the $X_{Si}Se_{Si}Si_{214}$ and $X_{Si}Te_{Si}Si_{214}$ compounds are almost identical to those observed for coimplanted Si compounds containing sulfur. This result occurs despite the fact that the different sized chalcogen atoms cause moderate variations in the resulting structures and energetics.

2. Optical properties

The effect of coimplantation on optoelectronic properties is shown in Fig. 9. The absorption coefficients of $X_{Si}S_{Si}Si_{214}$, $X_{Si}Se_{Si}Si_{214}$, and $X_{Si}Te_{Si}Si_{214}$ (X=B,Al) are represented. For the sake of clarity, only the most homogeneous arrangements of substituting atoms were analyzed because the distance between them does not considerably affect the electronic structure. Similarly to the results for the electronic properties, the absorption coefficient is almost independent of the use of B or Al. In both cases, the optical response persists for energies below the band gap.

However, as can be seen in the same figure, coimplantation reduces the optical absorption of photons with energies below the band gap of Si, when compared to the compounds implanted only with chalcogens. This drop can be explained by taking into account that the main peak is due to transitions between the IB and the CB. The partial occupancies of the IB after coimplantation lower the probabilities of most of these transitions and as a consequence a decrease in the peak around 0.8 eV is found.

In contrast, the optical excitation of electrons from the VB to the IB is now allowed. However, these transitions do not contribute to an increase in the absorption. This can be explained by representing the partial contributions to the total absorption. Figure 10 represents the imaginary part of the dielectric function of $B_{Si}S_{Si}Si_{214}$ separated into its partial contributions. The main peak centered at around 0.8 eV is due to transitions from the IB to the CB, whereas transitions
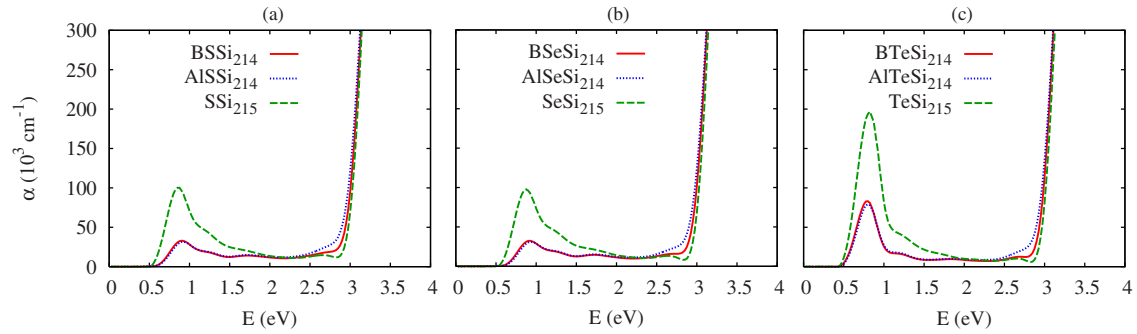
FIG. 9. (Color online) Optical absorption coefficients of (a) $X_{Si}S_{Si}Si_{214}$, (b) $X_{Si}Se_{Si}Si_{214}$, and (c) $X_{Si}Te_{Si}Si_{214}$ (with $X=$B and Al) compared to those of the compounds implanted only with chalcogens.

from the VB to the IB contribute mainly in the range 3–3.5 eV. The situation for any other combination of chalcogens and group III atoms is qualitatively the same: the main component always originates from transitions from the IB to the CB whereas transitions from the VB to the IB contribute to absorption mainly for photon energies closer to the Si direct band-gap edge.

IV. SUMMARY AND CONCLUSIONS

Substitutional implantation of S, Se, and Te chalcogen elements in silicon produces a band inside the host semiconductor band gap that is related to the impurity levels of these species. The electronic structure of $S_{Si}Si_{215}$, $Se_{Si}Si_{215}$, and $Te_{Si}Si_{215}$ compounds contains a band filled with two electrons (one per spin channel) that resembles to some degree the double-donor character of the chalcogen impurities. Due to the presence of this intermediate band, a high optical absorption is found for energies below the Si gap. A subband-gap absorption is also observed in experimental works of chalcogen-implanted Si.[16,17] In the case of Se implantation, Ref. [16] identified experimentally a peak in absorptance at 1800 nm, which agrees with the position of the absorption peak found in this work. In the case of Te, the subband-gap absorption is slightly stronger than for the other chalcogens.

The additional p-doping proposed for the aforementioned compounds allows the removal of part of the electron population from the band of the chalcogen-implanted Si, resulting in an intermediate band with the required properties. The presence of dopants does not significantly modify the other features of the electronic structure, such as the position or the width of the IB. This behavior is predicted for both boron and aluminum coimplantations.

The relative distance between the chalcogen and the introduced group III element is another factor that does not alter the main properties of the intermediate band. IB band properties are conserved even when the substitutions are carried out at next sites. When dopants and chalcogens are combined, a slight tendency toward next-site placement was observed, but this does not appear to spoil the intermediate-band features. It is worth highlighting that this trend is soft, although both atoms in principle could be oppositely charged, which may indicate the formation of a delocalized band rather than the combination of two charged impurities. The above tendency is smallest with B substitution.

Although subband gap optical absorption is reduced upon coimplantation because of a decrease in the magnitude of IB to CB transitions, experimentally measurable absorption persists in the graphs. In addition, after coimplantation, the transitions from the VB to the IB are allowed, although they contribute to absorption mainly for photon energies closer to the Si direct band-gap edge.

In conclusion, Si substitution with chalcogen elements at concentrations on the order of 0.5% can produce the features required for an intermediate-band material if this compound is additionally p doped. Two main factors favor the likelihood that this kind of material can be produced experimentally: first, the feasibility of combining a number of different chalcogens and doping elements; and second, the stability of the intermediate band against changes in the relative distance between substituting atoms. Because chalcogen-implanted Si has already been grown in crystalline form and p-type doping at similar concentrations is feasible for bulk Si, it is expected that experimental samples of these candidate intermediate-band materials will be synthesized relatively soon.
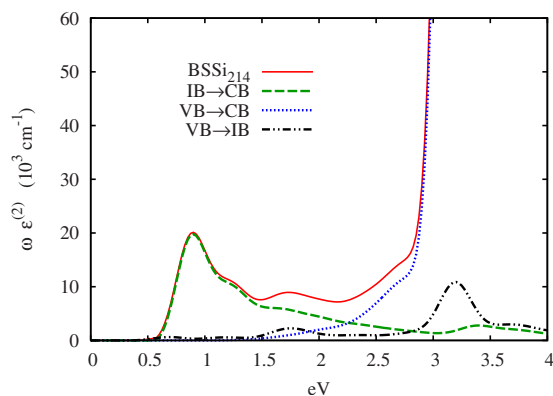

FIG. 10. (Color online) The imaginary part and its components of the dielectric function calculated for $B_{Si}S_{Si}Si_{214}$.

*Corresponding author; perla@etsit.upm.es

[1] J. Olea, M. Toledano-Luque, D. Pastor, G. González-Díaz, and I. Mártil, J. Appl. Phys. **104**, 016105 (2008).

[2] K. Sánchez, I. Aguilera, P. Palacios, and P. Wahnón, Phys. Rev. B **79**, 165203 (2009).

[3] A. Luque and A. Martí, Phys. Rev. Lett. **78**, 5014 (1997).

[4] P. Wahnón and C. Tablero, Phys. Rev. B **65**, 165115 (2002).

[5] P. Palacios, J. J. Fernández, K. Sánchez, J. C. Conesa, and P. Wahnón, Phys. Rev. B **73**, 085206 (2006).

[6] P. Palacios, K. Sánchez, J. C. Conesa, and P. Wahnón, Phys. Status Solidi A **203**, 1395 (2006).

[7] P. Palacios, I. Aguilera, K. Sánchez, J. C. Conesa, and P. Wahnón, Phys. Rev. Lett. **101**, 046403 (2008).

[8] I. Aguilera, P. Palacios, K. Sánchez, and P. Wahnón, Phys. Rev. B **81**, 075206 (2010).

[9] E. Antolín, A. Marti, J. Olea, D. Pastor, G. González-Díaz, I. Martil, and A. Luque, Appl. Phys. Lett. **94**, 042115 (2009).

[10] J. Olea, G. González-Díaz, D. Pastor, and I. Martil, J. Phys. D **42**, 085110 (2009).

[11] G. González-Díaz, J. Olea, I. Martil, D. Pastor, A. Marti, E. Antolin, and A. Luque, Sol. Energy Mater. Sol. Cells **93**, 1668 (2009).

[12] M. Sheehy, L. Winston, J. Carey, C. Friend, and E. Mazur, Chem. Mater. **17**, 3582 (2005).

[13] T. Kim, J. Warrender, and M. Aziz, Appl. Phys. Lett. **88**, 241902 (2006).

[14] M. Tabbal, T. Kim, J. M. Warrender, M. J. Aziz, B. L. Cardozo, and R. S. Goldman, J. Vac. Sci. Technol. B **25**, 1847 (2007).

[15] A. Luque, A. Martí, E. Antolín, and C. Tablero, Physica B **382**, 320 (2006).

[16] M. Tabbal, T. Kim, D. N. Woolf, B. Shin, and M. J. Aziz, Appl. Phys. A: Mater. Sci. Process. **98**, 589 (2010).

[17] M. A. Sheehy, B. R. Tull, C. M. Friend, and E. Mazur, Mater. Sci. Eng., B **137**, 289 (2007).

[18] P. Hohenberg and W. Kohn, Phys. Rev. **136**, B864 (1964).

[19] W. Kohn and L. J. Sham, Phys. Rev. **140**, A1133 (1965).

[20] G. Kresse and J. Hafner, Phys. Rev. B **47**, 558 (1993).

[21] G. Kresse and J. Furthmüller, Phys. Rev. B **54**, 11169 (1996).

[22] J. P. Perdew, J. A. Chevary, S. H. Vosko, K. A. Jackson, M. R. Pederson, D. J. Singh, and C. Fiolhais, Phys. Rev. B **46**, 6671 (1992).

[23] P. E. Blöchl, Phys. Rev. B **50**, 17953 (1994).

[24] G. Kresse and D. Joubert, Phys. Rev. B **59**, 1758 (1999).

[25] P. Pulay, Chem. Phys. Lett. **73**, 393 (1980).

[26] Y. Mo, M. Z. Bazant, and E. Kaxiras, Phys. Rev. B **70**, 205210 (2004).

[27] A. A. Taskin, Semiconductors **36**, 1083 (2002).

[28] M. Methfessel and A. T. Paxton, Phys. Rev. B **40**, 3616 (1989).

[29] J. Furthmüller, http://www.freeware.vasp.de/VASP/optics

[30] M. Gajdoš, K. Hummer, G. Kresse, J. Furthmüller, and F. Bechstedt, Phys. Rev. B **73**, 045112 (2006).

[31] M. W. Chase, C. A. Davies, J. R. Downey, Jr., D. J. Frurip, R. A. McDonald, and A. N. Syverud, in *JANAF Thermochemical Tables*, 3rd ed. [J. Phys. Chem. Ref. Data Suppl. **14**, 1 (1985)].

[32] E. Janzén, R. Stedman, G. Grossmann, and H. G. Grimmeiss, Phys. Rev. B **29**, 1907 (1984).

[33] J. Bernholc, N. O. Lipari, S. T. Pantelides, and M. Scheffler, Phys. Rev. B **26**, 5706 (1982).

[34] V. A. Singh, U. Lindefelt, and A. Zunger, Phys. Rev. B **27**, 4909 (1983).

[35] J. Coutinho, V. J. B. Torres, R. Jones, and P. R. Briddon, Phys. Rev. B **67**, 035205 (2003).

[36] G. W. Ludwig, Phys. Rev. **137**, A1520 (1965).

[37] H. G. Grimmeiss, E. Janzén, H. Ennen, O. Schirmer, J. Schneider, R. Wörner, C. Holm, E. Sirtl, and P. Wagner, Phys. Rev. B **24**, 4571 (1981).

[38] R. Hulstrom, R. Bird, and C. Riordan, Sol. Cells **15**, 365 (1985).